Communications in Science and Technology 10(1) (2025) 10–16

COMMUNICATIONS IN
SCIENCE AND TECHNOLOGY
Homepage: cst.kipmi.or.id

Biosynthesis of sulfur and selenium co-doped ZnO nanoparticles for the enhanced photocatalytic treatment of industrial wastewater

Ari Sulistyo Rini[a,*], Afrida Helena Sitorus[a], Yolanda Rati[b], Erman Taer[a], Zulkarnain Usman[a], Jasril[c], Akrajas Ali Umar[d]

[a] *Department of Physics, Faculty of Mathematics and Natural Science, Universitas Riau, Pekanbaru 28983, Indonesia*
[b] *Department of Physics, Faculty of Sciences, Institut Teknologi Sumatera, Lampung Selatan 35365, Indonesia*
[c] *Department of Chemistry, Faculty of Mathematics and Natural Science, Universitas Riau, Pekanbaru 28983, Indonesia*
[d] *Institute of Microengineering and Nanoelectronics (IMEN), Universiti Kebangsaan Malaysia, Bangi 43600, Malaysia*

Article history:
Received: 20 September 2024 / Received in revised form: 28 January 2025 / Accepted: 18 February 2025

Abstract

Although ZnO photocatalysts show potential for wastewater treatment, their low efficiency limits the commercialization. To address this problem, we investigated the effect of co-doping ZnO with selenium (4%, fixed) and sulfur (0.5, 1, and 1.5 wt%). The catalysts were synthesized using Matoa leaf extract and zinc nitrate hexahydrate while being subjected to 540 W microwave irradiation. UV-Vis analysis revealed absorption peaks at 340-398 nm with sulfur doping increasing the band gap. XRD confirmed the preservation of the hexagonal wurtzite structure, while FESEM images showed a morphological transformation from nanoflowers to petal flakes with increasing sulfur content. EDX analysis confirmed the presence of S, Se, Zn, and O, while FTIR analysis identified OH groups from the extract in the nanoparticles. BET surface area was found to progressively reduced from 24.58 to 16.86 m²/g with sulfur doping. The co-doped catalyst with 0.5 wt% sulfur (0.5S(4Se-ZnO)) demonstrated the highest degradation of 4-nitrophenol at 99.69%, indicating its applicability in industrial wastewater treatment. These findings indicate that the Se/S co-doped ZnO, prepared via a green synthesis route, holds a strong promise as an efficient and practical photocatalyst for addressing environmental pollution in a sustainable and economical manner.

Keywords: Degradation; Matoa leaf; S,Se co-doped ZnO; pollutant 4-nitrophenol

1. Introduction

In recent years, water pollution has emerged as a global crisis, driven by rapid economic growth and industrial expansion. The growth of textile industry becomes a crucial factor that contributes to environmental degradation [1]. The production process in this sector generate liquid waste, which poses serious risks to both environmental and human health if not properly treated [2]. One prevalent industrial pollutant in wastewater is nitroaromatic compounds, such as 4-nitrophenol. The Environment Protection Agency (EPA) has classified 4-nitrophenol, due to its high solubility and stability, as a hazardous pollutant that can have detrimental effects on human health [3]. The decomposition of 4-nitrophenol is therefore deemed crucial for addressing environmental issues and sustaining ecosystems.

Various techniques, including catalytic conversion [4], carbon adsorption [5], catalytic hydrogenation [6], and electrolysis [7] have been employed to facilitate the decomposition of 4-NP pollutants. Among of these techniques, photocatalytic degradation is the most effective in view of its low cost, rapid degradation time, and environmentally friendly nature [8]. Photocatalytic methods are typically developed by means of light-responsive semiconductor catalysts with ZnO, TiO_2, Fe_2O_3, CuO and SnO_2 being the most widely studied [9], [10-13]. In particular, ZnO has attracted attention as a photocatalyst due to its non-toxic nature and high redox potential, making it as a promising material [14]. However, its wide band gap energy (3.37 eV) results in relatively low photocatalytic activity due to fast charge carrier recombination and low photon efficiency [15]. For this, further ZnO modification is required for the improvement of the photocatalytic efficiency.

Doping ZnO semiconductors with nonmetals narrow the band gap energy, which is beneficial for photocatalytic activity [16]. Research by Taha et al. showed that the addition of Se to ZnO could improve electron transfer from the conduction band to the valence band (3.15 eV), facilitating the formation of reactive oxygen species [17]. Other studies have also demonstrated that doping ZnO with S could form an intermediate energy level, allowing for greater light absorption

---

* Corresponding author.
Email: ari.sulistyo@lecturer.unri.ac.id
https://doi.org/10.21924/cst.10.1.2025.1539

and reducing electron-hole pair recombination [9]. Motivated by the improvement of the photocatalytic performance of nonmetal monodoped ZnO, this study in turn explored the co-doping of ZnO with two nonmetals (S and Se) to further enhance its photocatalytic performance in degrading organic pollutants. Several studies have reported combinations dual nonmetal for co doping ZnO such as S, C, N, and F elements with band gap energy (S,C)ZnO of 3.13 eV and (N,F)ZnO of 3.23 eV [18,19]. Whereas, studies with the co-doping of S and Se, so far, have not been reported. Therefore, selenium (Se) and sulfur (S) are chosen as dopants to enhance the photocatalytic performance of zinc oxide (ZnO) considering their ability to improve visible-light absorption, reduce charge carrier recombination, and increase the generation of reactive oxygen species that are crucial for the degradation of organic pollutants.

As conventional method in ZnO synthesis often involves toxic chemicals, complex equipment, and stringent experimental conditions, we then opted for a microwave-assisted biosynthesis approach. This method is able to offer rapid heating, cost-effectiveness, consistent nanoparticle production, and ability to control nanoparticle purity [20]. Biosynthesis provides a sustainable and efficient alternative for any conventional synthesis methods with significant advantages in terms of environmental impact and technical capabilities [21]. It is particularly effective for incorporating elements such as sulfur and selenium into materials, enhancing their properties for various applications. Plant extracts play a critical role in biosynthesis, utilizing phytochemicals (terpenoids, polyphenols, tannins, and saponins) capable of bio-reducing nanoparticles [22]. Notably, the synergistic effects of Se and S co-doping on ZnO via this method for photocatalytic applications, so far, have not been previously explored. In this study, we reported the microwave-assisted biosynthesis of S, Se co-doped ZnO using Matoa leaf extract as a reducing agent and analyzed the synergistic effect of S and Se co-doping on ZnO in the photocatalytic degradation of 4-nitrophenol. Matoa leaf was chosen for this research for its availability in campus as well as affordability.

2. Experimental Methods

2.1. Materials

Matoa leaf extract, zinc nitrate hexahydrate ($Zn(NO_3)_2.6H_2O$; HIMEDIA®), sodium borohydride ($NaBH_4$; 97% Extra Pure Loba Chemie), Selenium powder (99.9% Loba Chemie), 4-nitrophenol ($C_6H_5NO_3$ or 4-NP; Sigma-Aldrich), sodium hydroxide (NaOH; EMSURE®), hydrogen peroxide (50% H_2O_2) were purchased from analytical grade and utilized without any further treatment. Deionized (DI) water was used as a solvent for the whole time of the experiment.

2.2. Biosynthesis of Se-ZnO and S, Se-ZnO

Matoa leaf extract was prepared by following the method from our previous study [23]. Matoa leaf extract, rich in phenolic compounds, particularly vanillin, phenol, and benzene, became the major ingredient. These compounds, along with flavonoids and other secondary metabolites such as tannins and saponins, contribute to the extract's potential health benefits, including antioxidant and antimicrobial activities. To synthesize Se-doped ZnO (Se-ZnO), a solution containing 0.05 M zinc nitrate hexahydrate, 0.02 g/mL Matoa leaf extract, and 0-50 mM selenium solution was stirred until being homogeneous. The mixture was then irradiated in a microwave oven at 540 W for 3 minutes, centrifuged at 4000 rpm and dried at 110ºC for 30 minutes. For S, Se co-doped ZnO, Na_2S solution was added at different weight percentages (0.5, 1, and 1.5wt%) using a similar process. Finally, the resulted co-doped samples were labeled as 4Se-ZnO, 0.5S(4Se-ZnO), 1.0S(4Se-ZnO), and 1.5S(4Se-ZnO).

2.3. Characterization

The UV-Vis absorption was measured using an Agilent Cary 60 spectrophotometer in the range of 200 to 800 nm. The crystal structure was characterized by X-ray diffraction (XRD) using a Rigaku Miniflex 600 Benchtop with Cu-Kα radiation ($\lambda = 1.5406$ Å) at $2\theta = 20$-$80°$. Further, surface morphology was examined by means of a JSM-IT700HR Field Emission Scanning Electron Microscope (FESEM) at 25,000x magnification. The surface area and pore volume of S, Se-ZnO were determined by nitrogen adsorption using a Brunauer-Emmett-Teller (BET) Quatntachrome Novatouch LX-4 at a degassing temperature of 300°C. Fourier-transform infrared (FTIR) spectra were recorded with a Shimadzu IR Prestige-21 in the range of 400-4000 cm⁻¹.

2.4. Photocatalysis test

0.01 g of Se-ZnO and S(Se-ZnO) samples were added to a 4-NP solution and homogenized for 60 minutes in the dark to ensure adsorption-desorption equilibrium. Subsequently, photocatalytic activity was investigated under 8-watt UV-C lamps. Samples of 5 mL were taken every 10 minutes over an 80-minute period to observe any changes in the 4-NP pollutant. Here, the concentration reduction of 4-NP was monitored by means of UV-Vis spectroscopy, and the degradation percentage was calculated with the following equation:

$$\%\ \text{Degradation} = \frac{(A_0 - A)}{A_0} \times 100\% \qquad (1)$$

where A_0 and A refer to the initial and final absorbance, respectively [9]

3. Results and Discussion

3.1. Optical properties

Fig. 1 illustrates the UV-Vis absorption spectra of Matoa leaf extract, Se-doped ZnO, and S,Se co-doped ZnO and bandgap energy approximation. The maximum absorption of Matoa leaf extract was observed at a wavelength of 279 nm, consistent with previous studies by Yudasari et al., reporting peaks between 242285 nm [14].

The absorption peak of Se-ZnO and S(Se-ZnO) samples was observed in the UV region at 340-398 nm. Our previous study reported the absorption peak of ZnO pristine at 359 nm with bandgap 3.13 eV [24]. This characteristic is aligned with findings by Robles et al. who recorded similar absorption ranges for green-synthesized ZnO in the range of 320 to 400 nm [25]. The increase in sulfur co-dopant concentration in 4Se-ZnO exhibited the redshift with the peak shifts from 368 nm to 377 nm for 1.5S(4Se-ZnO) sample. The addition of a sulfur led to an improved longer light absorption attributed to the alteration of the electronic structure caused by sulfur, thereby broadening the absorption spectrum [9].

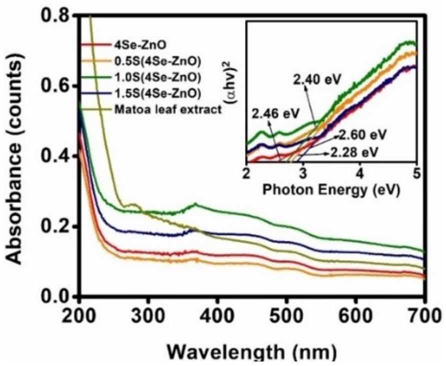

Fig. 1. (a) The absorption spectrum; (b) bandgap energy of Matoa leaf extract, 4Se-ZnO, and S(4Se-ZnO) at different wt% of S

The inset in Fig. 1 shows the band gap energies of 4Se-ZnO and S(Se-ZnO) samples, calculated using the *Tauc Plot* method. The bandgap energies for 4Se-ZnO, 0.5S(4Se-ZnO), 1.0S(4Se-ZnO), and 1.5S(4Se-ZnO) were 2.46, 2.28, 2.40, and 2.60 eV, respectively. These results showed that the addition 0.5% of sulfur to the 4Se-ZnO system decreased the band gap energy. It can be attributed to sulfur's incorporation into the interstitial lattice of the 4Se-ZnO nanoparticles [9]. However, increasing the S content to 1% in 4Se-ZnO resulted in an increase in band gap energy close to Se-ZnO. It suggests that S-doping induces defect states and oxygen vacancies in the ZnO lattice, enhancing charge carrier separation and decreasing electron-hole recombination, even at elevated band gap energies. Co-doping of sulfur and selenium might yield a synergistic effect optimizing the electronic structure of zinc oxide, enhancing visible light absorption, and increasing charge carrier mobility. 1.5%S doping can increase an energy band gap and may improve the overall photoactivity of the material when combined with Se, as demonstrated in prior research on nonmetal doping pairs such as S-C or N-F [26]. Alterations in absorption characteristics and band gap energy suggest that sulfur co-doping is markedly able to enhance the material's efficacy as a photocatalyst.

3.2. Structural analysis

Fig. 2 shows the XRD patterns of 4Se-ZnO and S(4Se-ZnO) at different sulfur concentration. Nine diffraction peaks matched the ZnO database (COD No. 969004180), appearing at 2θ values of 31.72º, 34.38º, 36.51º, 47.49º, 56.55º, 62.83º, 66.51º, 67.91º, 69.04º. These peaks correspond to the hexagonal wurtzite structure with diffraction planes (100), (002), (101), (200), (102), (110), (112) and (201). The XRD pattern is consistent with the previous work by Aga et al. who used sol-gel method for Se-ZnO synthesis [16]. This shows that microwave-assisted biosynthesis can yield similar crystallinity and structure as chemical conventional methods. Here, there was no significant change in crystallinity and phase occurred during the co-doping process, as evidenced sharp and narrow peak.

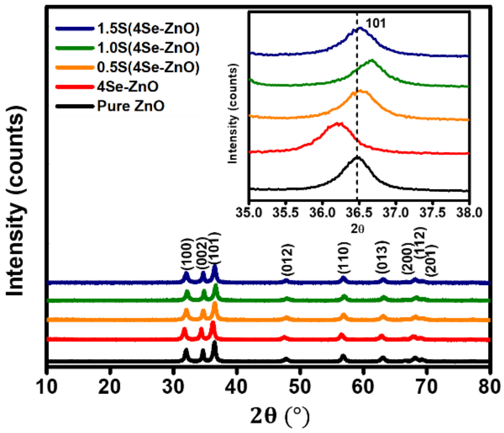

Fig. 2. (a) XRD pattern; (b) The maximum peak (101) of 4Se-ZnO and S(4Se-ZnO) at different wt% of S

The inset in Fig. 2 shows the magnified view of the highest diffraction peaks at (101) of the 4Se-ZnO and S(4Se-ZnO) samples. A noticeable peak shift observed indicated a change in atomic spacing. This shift was determined by the atomic radius differences among S, Zn, and Se atoms with atomic radii of S (1.84 Å) > Zn (0.74 Å) > Se (0.5 Å) [27]. Due to the significant difference in atomic radii, sulfur atoms were not able to substitute for Se and Zn atoms in the 4Se-ZnO crystal structure. Instead, S atoms occupied interstitial positions within the crystal lattice between the Se atoms [28]. Interstitial atoms are located in the gaps or empty spaces between the main atoms in a crystal structure, and their presence then affects atomic distances, thereby causing the observed peak shift to a higher angle [29].

Tabel 1. Parameter XRD of 4Se-ZnO and S(4Se-ZnO) at different wt% of S

Sample (wt%)	2θ (º)	Lattice constant		FWHM (º)	Crystallite size (nm)
		a (Å)	c (Å)		
4Se	36.191	0.634	3.25	5.21	13.17
0.5S,4Se	36.511	0.653	3.22	5.16	12.80
1.0S,4Se	36.634	0.633	3.21	5.14	13.21
1.5S,4Se	36.495	0.648	3.22	5.16	12.89

Table 1 presents the lattice parameters and crystallite sizes of 4Se-ZnO and S(4Se-ZnO) at various sulfur weight percentages. The lattice parameters (a and c) of the hexagonal wurtzite structure were calculated using Eq. (2):

$$d_{hkl} = \left[\frac{4(h^2+hk+k^2}{3a^2} + \left(\frac{l}{c}\right)^2\right]^{-\frac{1}{2}} \tag{2}$$

Meanwhile, the crystallite sizes of the Se-ZnO and S,Se-ZnO samples were determined using the Debye-Scherrer equation, as shown in Eq. (3):

$$D = \frac{0.9\lambda}{\beta_{hkl} cos\theta} \tag{3}$$

where d, hkl, λ, θ are the interplane spacing, Miller indices, wavelength (1.541 Å), and Bragg angle, respectively.

The 4Se-ZnO sample exhibited a crystallite size of 13.17 nm. Upon the addition of 0.5 wt% sulfur (0.5S(4Se-ZnO)), the crystallite size slightly decreased to 12.80 nm. In 1.0S(4Se-ZnO), the crystallite size again increased to 13.21 nm prior to reduce to 12.89 nm in 1.5S(4Se-ZnO). This variation in crystallite size is attributed to the co-doping process, where the introduction of sulfur at different weight percentages causes lattice distortion and is influenced by the atomic radius differences between the dopants and Zn atoms [28]. Talukdar et al. stated that smaller crystallite sizes can positively impact photocatalytic activity [30]. This is because smaller crystallites typically feature more defects or vacancies, which serve as active sites or trap centers, effectively reducing charge carrier recombination and increasing photocatalytic activity.

3.3. FESEM-EDX analysis

Fig. 3(a) shows the morphology of 4Se-ZnO nanoparticles, exhibiting a flower-like structure with clearly distinguishable cores and petals. For co-doped S(4Se-ZnO) samples in Fig. 3(b-d), the particles maintained the flower-shaped morphology, but with smaller and more uniform sizes compared to 4Se-ZnO, as shown in the histogram next to the morphology. The particle sizes for 4Se-ZnO, 0.5S(4Se-ZnO), 1.0S(4Se-ZnO), and 1.5S(4Se-ZnO) were measured at 241, 207, 187, and 193 nm, respectively.

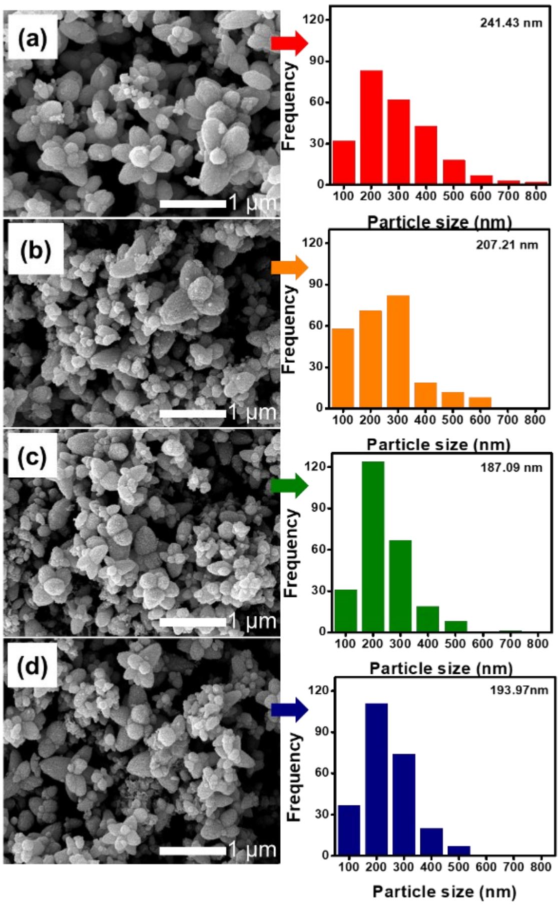

Fig. 3. Surface morphology of: (a) 4Se-ZnO; (b) 0.5S(4Se-ZnO); (c) 1.0 S(4Se-ZnO); (d) 1.5 S(4Se-ZnO)

The particle size analysis revealed a significant reduction in particle size with S co-doping, particularly for 1.0S(4Se-ZnO), and 1.5S(4Se-ZnO). This indicated that S incorporation promoted a finer particle size distribution, likely due to improved control over nucleation and growth during synthesis. In addition, the sulfur as co-dopant to 4Se-ZnO nanoparticles reduced particle size and increased uniformity without altering the basic flower-like shape. In a study by Qu et al., flower-shaped nanoparticles exhibited a better photocatalytic performance compared to nanorod-shaped ones [31]. It is due to the larger surface area and the formation of empty spaces that acted as the active sites.

Fig. 4 presents EDX spectrum confirming the presence of Zn, O, Se, and S elements. Here, the Zn and O elements provided the highest intensities for all samples, indicating their dominance in the doped and co-doped nanoparticles. While, the Se elements showed the lowest intensity, and the S element was undetected. This absence of sulfur may be due to the low acceleration voltage applied to the sample during EDX measurement, which was insufficient for detecting certain elements. A similar observation was reported by Sahdiah et al., where elements such as, Mg, K, and Ca were also undetected due to similar reason with detection sensitivity [32].

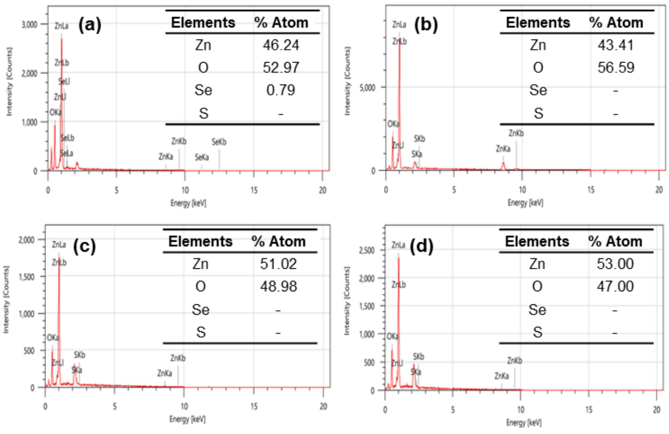

Fig. 4. EDX spectrum of: (a) 4Se-ZnO; (b) 0.5S(4Se-ZnO); (c) 1.0 S(4Se-ZnO); (d) 1.5 S(4Se-ZnO)

3.4. FTIR studies

Fig. 5 depicts the FTIR spectrum of 4Se-ZnO and S(4Se-ZnO) samples, displaying the functional groups in their bending and stretching modes across the 500-4000 cm^{-1} range. The functional groups identified in all samples were almost similar. A broad and strong O-H stretching band was observed between 3500 and 4000 cm^{-1} in all samples, in accordance with findings of Chauhan et al. who reported O-H stretching in a similar range [33].

The peak at 2100 cm^{-1} corresponded to the presence of C=C alkyne group, while the peak at 1900 cm^{-1} indicated C=O carbonyl functional group. ZnO NPs were identified by a transmission band in the region between 500 and 600 cm^{-1} corresponding to the hexagonal crystal structure of ZnO. The peak observed at 860 cm^{-1} was associated with the Se-O vibration. This result aligns with the previous report that found Se-O vibration at 880 cm^{-1} in biosynthesized Se-doped ZnO [34]. Additionally, a new peak appeared in the sulfur-doped sample around 1300-1400 cm^{-1}, indicating the formation of a Zn-S microstructure during the doping process [16].

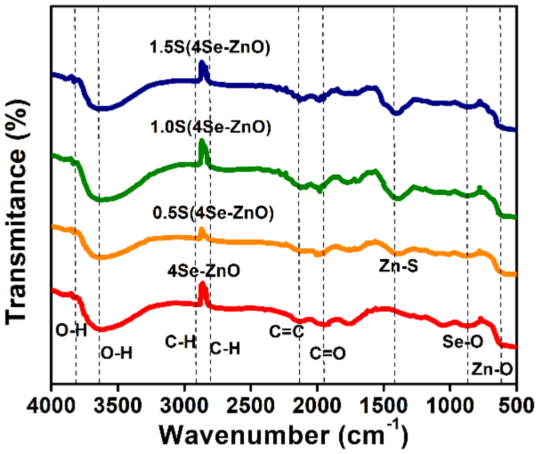

Fig. 5. FTIR spectrum of 4Se-ZnO and S(4Se-ZnO) at different wt% of S

3.5. BET analysis

Fig. 6 presents the nitrogen adsorption-desorption isotherms of Se-ZnO and S(Se-ZnO) samples, measured using BET. The results revealed a type IV isotherm curve with H_2 hysteresis loop in the IUPAC classification (International Union of Pure and Applied Chemistry [17]. In the 4Se-ZnO sample, the adsorption isotherm curve showed a closed characteristic, typically indicating that the adsorption reached a saturation point, possibly due to a uniformly distributed pore structure or the presence of micropores. However, when sulfur was co-doped into 4Se-ZnO, the isotherm curve changed to an open characteristic – indicating an increase in the adsorption capacity or a significant change in the pore structure. Table 2 presents the surface area, pores volume, and pores size data of Se-ZnO and S(Se-ZnO) nanoparticles.

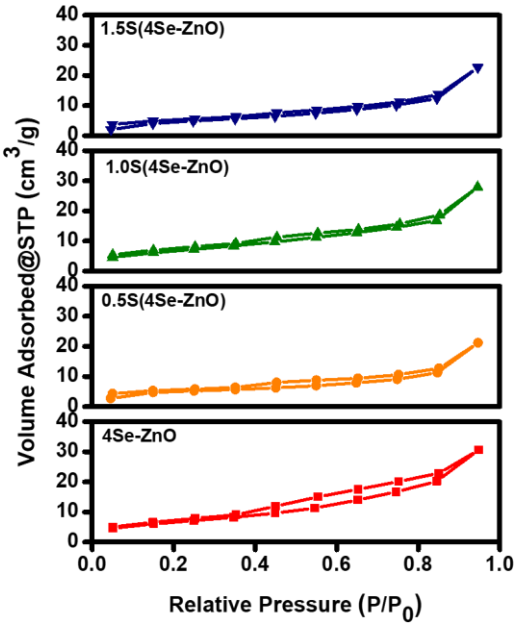

Fig. 6. The absorption-desorption isotherm of 4Se-ZnO and S(4Se-ZnO) at different wt% of S

Tabel 2. Surface area, pores volume, and pores size 4Se-ZnO and S(4Se-ZnO)

Sample name	Surface area (m^2/g)	Pore volume (cm^3/g)	Pore size (nm)
4Se-ZnO	16.86	3.90	0.033
0.5S(4Se-ZnO)	24.58	3.52	0.047
1.0S(4Se-ZnO)	17.38	4.04	0.035
1.5S(4Se-ZnO)	24.20	3.93	0.043

The 0.5S(4Se-ZnO) and 1.5S(4Se-ZnO) samples showed the largest BET surface areas of 24.58 m^2/g and 24.20 m^2/g, respectively. The largest pore size was found in the 0.5S(4Se-ZnO) sample (0.047 nm), which may facilitate more efficient reactant diffusion. Meanwhile, 1.0S(4Se-ZnO), with a slightly smaller pore size (0.035 nm), had the highest pore volume (4.04 cm^3/g), contributing to increased reactant adsorption capacity. In contrast, 4Se-ZnO had the smallest pore size (0.033 nm) and relatively low pore volume (3.90 cm^3/g), which may limit its photocatalytic activity. The surface area, pore volume, and pore size measurements indicated that S co-doping did not significantly influence the pore structure of Se-ZnO. The observed variations in surface area were likely due to localized surface modifications caused by S incorporation. This finding suggested that the enhanced photocatalytic activity emerged from changes in the material's electronic properties and surface chemistry, rather than alterations in porosity [35]. The relationship between crystallite size and surface area, as observed by XRD, was correlated. A combination of small crystallite sizes with mesoporous pores often yields superior photocatalytic performance as larger pore volume is beneficial in adsorbing more organic pollutant molecules [9].

3.6. Photocatalytic activity

Fig. 7(a) shows the absorbance peak of 4-NP (4-nitrophenol) degraded using 4Se-ZnO as a catalyst. The maximum absorbance peak of 4-NP was observed at a wavelength of 406 nm [36]. As the irradiation time increased, the absorbance decreased, eventually disappearing after 60 minutes. This reduction in absorbance occurred when the photon energy received by the photocatalyst exceeded its bandgap energy. When the photon energy was sufficient to activate the ZnO photocatalyst, electron-hole pairs were generated, triggering redox reaction producing reactive radical species, such as hydroxyl radicals (•OH). These radicals attacked 4-NP molecules, oxidizing and decomposing them into simpler products, leading to a decrease in 4-NP concentration over time. The disappearance of the absorbance peak after 60 minutes indicated the significant or complete degradation of 4-NP [37].

Fig. 7(b) shows a graph of the (A/A_0) ratio versus time, where A is the absorbance at a given time, and A_0 is the initial absorbance. The 4Se-ZnO sample demonstrated rapid initial degradation, but the rate slowed over time. With sulfur doping, the initial degradation rate slowed, yet the 0.5S(4Se-ZnO) sample overall achieved the most efficient degradation. The 1.0S(4Se-ZnO) and 1.5S(4Se-ZnO) samples also exhibited effective degradation with a steady rate and a low A/A_0 value by the end of experiment. The ln (A/A_0) value indicated the reaction rate constant analyzed using the pseudo-first-order approach [25]. Table 3 presents the summary of the reaction rate and degradation percentage values.

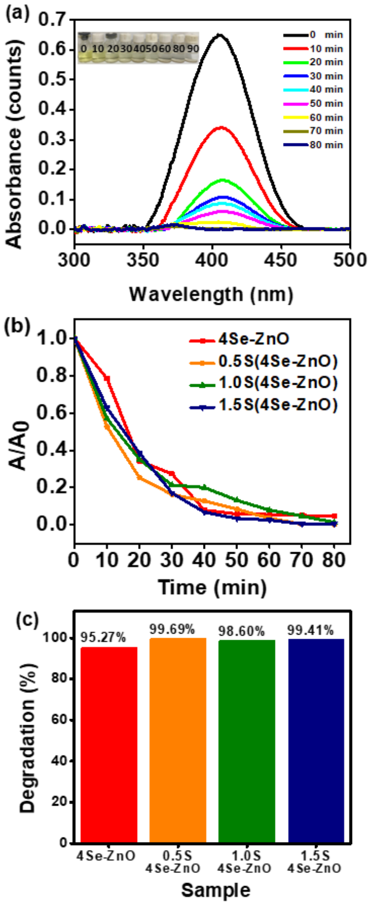

Fig. 7. (a) Absorbance spectrum with inset degradation process of 4-NP pollutant; (b) ln (A/A_0) vs time; (c) photocatalytic efficiency of 4Se-ZnO and S(4Se-ZnO) at different wt% of S

Tabel 3. Reaction rate and % degradation of 4Se-ZnO and S(4Se-ZnO) at different wt% of S

Sample name	Reaction rate (min^{-1})	Degradation percentage (%)
4Se-ZnO	-0.042	95.27
0.5S(4Se-ZnO)	-0.070	99.69
1.0S(4Se-ZnO)	-0.046	98.60
1.5S(4Se-ZnO)	-0.069	99.41

The addition of sulfur co-dopant to 4Se-ZnO significantly improved the photocatalytic efficiency, as evidenced by the increasing reaction rate constant and degradation percentage for all sulfur-doped samples compared to 4Se-ZnO. Among of these, the 0.5S(4Se-ZnO) sample exhibited the highest reaction rate constant (-0.070 min^{-1}) and degradation percentage (99.69%), indicating that sulfur co-doping at this concentration was highly effective in accelerating the degradation reaction and maximizing the photocatalytic efficiency. Similarly, the 1.5S(4Se-ZnO) sample also had an excellent performance with a reaction rate constant of -0.0690 min^{-1} and a degradation of 99.41%. Whereas, the 1.0S(4Se-ZnO) had a slightly lower reaction rate constant (-0.0464 min^{-1}) and degradation percentage (98.60%). In contrast, the undoped 4Se-ZnO exhibited the lower reaction rate constant (-0.0424 min^{-1}) and a degradation percentage of 95.27% degradation. A comparative study by Taha et al. showed a reaction rate of -0.0032 min^{-1} on methylene blue with a only 70% degradation after 240 minutes [17]. Small changes in the morphology, microstructure and porosity of Se-ZnO due to S co-doping indicated that the enhanced photocatalytic activity was primarily driven by electronic and surface chemical modifications rather than structural changes [38]. The co-doping process worked synergistically to fine-tune the bandgap, increased oxygen vacancies, and improved charge carrier separation, leading to a notable 4% boost in photocatalytic efficiency compared to bare Se-ZnO. These finding demonstrated the important role of sulfur co-dopant in improving the photocatalytic performance of 4Se-ZnO with the 0.5S(4Se-ZnO) showing the most optimal performance.

4. Conclusion

This work aimed to report the use of Matoa leaf extract for microwave-assisted biosynthesis co-doping ZnO with elemental selenium and sulfur. The synthesis method was straightforward and simple, producing a photocatalyst highly efficient of degrading 4-NP pollutants. Optical analysis demonstrated a red shift and a reduction in band gap energy for 4Se-ZnO when sulfur was added as co-dopant. XRD results confirmed a hexagonal wurtzite crystal structure, primarily along the (101) plane. Meanwhile, FESEM images revealed nanoflower shaped particles, while FTIR analysis corroborated the presence of functional groups on the surface of ZnO co-doped nanoparticles. Both FTIR and BET analysis further validated these findings, revealing new functional groups and an increased surface area. Consequently, from this study it can be concluded that sulfur co-doping in 4Se-ZnO can significantly enhance the photocatalyst's activation for the degradation of industrial pollutants.

Acknowledgements

The authors thank the Directorate General of Research and Community Service, Ministry of Higher Education, Science, and Technology, Republic of Indonesia for funding support. Appreciation is also extended to the Institute for Research and Community Service, Universitas Riau for their continual support throughout this project.

References

1. J. Rapsikevičienė, I. Gurauskienė, and A. Jučienė, *Model of industrial textile waste management*, Environ. Res. Eng. Manag, (2019) 43–55.
2. Khan., Sana., and A. Malik, *Toxicity evaluation of textile effluents and role of native soil bacterium in biodegradation of a textile dye*, Environ. Sci. Pollut. Res. 25 (2018) 4446–4458.
3. I. Ibrahim *et al.*, *Photocatalysis as an advanced reduction process (ARP): The reduction of 4-nitrophenol using titania nanotubes-ferrite nanocomposites*, J. Hazard. Mater. 372 (2019) 37–44.
4. M. Bagheri, M. Y. Masoomi, A. Forneli, and H. García, *A Quasi-Metal–*

Organic Framework Based on Cobalt for Improved Catalytic Conversion of Aquatic Pollutant 4-Nitrophenol, J. Phys. Chem. C. 126 (2022) 683–692.

5. X. Yang *et al.*, *Cotton-derived carbon fiber-supported Ni nanoparticles as nanoislands to anchor single-atom Pt for efficient catalytic reduction of 4-nitrophenol*, Appl. Catal. A Gen. 643 (2022) 118734.
6. T. Elysabeth, E. L. Dewi, Ratnawati, K. Mulia, and Slamet, *Simultaneous photoelectrocatalytic hydrogen production and ammonia degradation using titania nanotube-based photoanodes,* Commun. Sci. Technol. 9 (2024) 207–218.
7. Q. Wang, W. Wang, C. Zhu, C. Wu, and H. Yu, *A novel strategy to achieve simultaneous efficient formate production and p-nitrophenol removal in a co-electrolysis system of CO_2 and p-nitrophenol*, J. CO_2 Util. 47 (2021).
8. M. Chandhru *et al.*, *Bio-fabricated silver nanocatalyst for photocatalytic degradation and organic transformation of toxic pollutants*, Next Mater. (2023) 100023.
9. Z. Mirzaeifard, Z. Shariatinia, M. Jourshabani, and S. M. Rezaei Darvishi, *ZnO Photocatalyst Revisited: Effective Photocatalytic Degradation of Emerging Contaminants Using S-Doped ZnO Nanoparticles under Visible Light Radiation*, Ind. Eng. Chem. Res. 59 (2020) 15894–15911.
10. R. K. Shah, *Efficient photocatalytic degradation of methyl orange dye using facilely synthesized α-Fe_2O_3 nanoparticles*, Arab. J. Chem. 16 (2023).
11. A. A. Kassem, H. N. Abdelhamid, D. M. Fouad, and S. A. Ibrahim, *Catalytic reduction of 4-nitrophenol using copper terephthalate frameworks and CuO@C composite*, J. Environ. Chem. *Eng.* 9 (2021).
12. M. R. Kumar, G. Murugadoss, N. Venkatesh, and P. Sakthivel, *Synthesis of Ag_2O-SnO_2 and SnO_2-Ag_2O Nanocomposites and Investigation on Photocatalytic Performance under Direct Sun Light*, ChemistrySelect. 5 (2020) 6946–6953.
13. W. M. Naufal, S. Wahyuningsih, and W. W. Lestari, *Investigation of hexanal removal through adsorption and photocatalysis on ZIF-7 modified with ZnO, TiO_2, and ZnO/TiO_2 using ATR-FTIR*, Commun. Sci. Technol. 9 (2024) 235–242.
14. N. Yudasari, P. A. Wiguna, W. Handayani, M. M. Suliyanti, and C. Imawan, *The formation and antibacterial activity of Zn/ZnO nanoparticle produced in Pometia pinnata leaf extract solution using a laser ablation technique*, Appl. Phys. A Mater. Sci. Process. 127 (2021).
15. M. Elias *et al.*, *A highly efficient and stable photocatalyst; N-doped ZnO/CNT composite thin film synthesized via simple sol-gel drop coating method*, Molecules. 26 (2021).
16. K. W. Aga, M. T. Efa, and T. T. Beyene, *Effects of Sulfur Doping and Temperature on the Energy Bandgap of ZnO Nanoparticles and Their Antibacterial Activities,* ACS Omega.7 (2022) 10796–10803.
17. K. K. Taha, M. M. Mustafa, H. A. M. Ahmed, and S. Talab, *Selenium Zinc Oxide (Se/ZnO) Nanoparticles: Synthesis, Characterization, and Photocatalytic Activity*, Zeitschrift fur Naturforsch. - Sect. A J. Phys. Sci., (2019)
18. K. Dib, M. Trari, and Y. Bessekhouad, *(S,C) co-doped ZnO properties and enhanced photocatalytic activity*, Appl. Surf. Sci. 505 (2020).
19. K. Ayeb, N. Moussa, M. F. Nsib, S. G. Leonardi, and G. Neri, *NO_2 sensing properties of N-, F-, and NF co-doped ZnO nanoparticles,* Mater. Sci. Eng. B. 263 (2021) 114870.
20. F. Sujatmiko, I. Sahroni, G. Fadillah, and I. Fatimah, *Visible light-responsive photocatalyst of SnO_2/rGO prepared using Pometia pinnata leaf extract*, Open Chem. 19 (2021) 174–183.
21. T. D. Nguyen, T. P. Nguyen, N. T. Thai, and Y. H. Hoang, *Investigating the antimicrobial activity of silver nanoparticles with varying charges green-synthesized from Tabebuia rosea flower*, Commun. Sci. Technol. 9 (2024) 398–410.
22. Mejía, Y. Rodriguez, R. Bogireddy, and N. Kumar, *Reduction of 4-nitrophenol using green-fabricated metal nanoparticles*, RSC Advances. 12 (2022) 18661–18675.
23. Rini, Ari Sulistyo, Y. Rati, R. Dewi, and S. Putri, *Investigating the Influence of Precursor Concentration on the Photodegradation of Methylene Blue using Biosynthesized ZnO from Pometia pinnata Leaf Extracts*, *Baghdad Sci. J.* 20 (2023) 2532–2539.
24. A. S. Rini, Y. Rati, G. Maheta, A. P. Aji, and Saktioto, *Utilizing Pometia Pinnata leaf extract in microwave synthesis of ZnO nanoparticles: Investigation into photocatalytic properties*, Commun. Sci. Technol. 9 (2024) 94–99
25. S. C. A. Robles *et al.*, "Biosynthesis, characterization and photocatalytic activity of ZnO nanoparticles using extracts of Justicia spicigera for the degradation of methylene blue," *J. Mol. Struct.*, 1225 (2021).
26. A. Joy *et al.*, *Solar photocatalysts: non-metal (C, N, and S)-doped ZnO synthesized through an industrially sustainable in situ approach for environmental remediation applications,* RSC Adv. 14 (2024) 21655–21667, 2024.
27. N. Chauhan, V. Singh, S. Kumar, M. Kumari, and K. Sirohi, *Synthesis of sulphur & indium co-doped mesoporous zinc oxide nanoparticles via hydrothermal method to study their photocatalytic activity*, Optik (Stuttg). 185 (2019) 838–846.
28. Rini., A S., R. Dewi, R. Asriani, and Y. Rati, *Biosynthesis of sulfur-doped zinc oxide using bidara leaf extract,* in *Journal of Physics: Conference Series*, 2596 (2023).
29. Y. Li, L. L. Chen, X. X. Lian, and J. Li, *Formation Mechanism and Gas-Sensing Performance of La/ZnO Nanoplates Synthesized by a Facile Hydrothermal Method*, J. Electron. Mater. 47 (2018) 2970–2978.
30. Talukdar, R. K. Dutta, and Soumita, *A mechanistic approach for superoxide radicals and singlet oxygen mediated enhanced photocatalytic dye degradation by selenium doped ZnS nanoparticles*, RSC Adv. 6 (2016) 928–936.
31. Y. Qu, R. Huang, W. Qi, M. Shi, R. Su, and Z. He, *Controllable synthesis of ZnO nanoflowers with structure-dependent photocatalytic activity*, Catal. Today. 355 (2020) 397–407.
32. Sahdiah, Halimahtus, and R. Kurniawan, *Optimasi Tegangan Akselerasi pada Scanning Electron Microscope – Energy Dispersive X-Ray Spectroscopy (SEM-EDX) untuk Pengamatan Morfologi Sampel Biologi*, J. Sains dan Edukasi Sains. 6 (2023) 117–123.
33. N. Chauhan, V. Singh, S. Kumar, and R. L. Dhiman, *Influence of Nickel, Silver, and Sulphur Doping on the Photocatalytic Efficiency of Mesoporous ZnO Nanoparticles*, Arab. J. Sci. Eng. 45 (2020) 249–259.
34. A. Majeed *et al.*, *Green synthesized selenium doped zinc oxide nano-antibiotic: synthesis, characterization and evaluation of antimicrobial, nanotoxicity and teratogenicity potential*, *J. Mater. Chem. B.* 8 (2020) 8444–8458.
35. H. Wu *et al.*, *Drinking-bird-enabled triboelectric hydrovoltaic generator, Device,* 2 (2024) 100318, 2024.
36. A. Sulistyo, A. Purnomo, and Y. Rati, *Microwave-assisted biosynthesis of flower-shaped ZnO for photocatalyst in 4-nitrophenol degradation,* Commun. Sci. Technol. 7 (2022) 135–139.
37. E. O. Ichipi, A. B. Mapossa, A. C. F. M. Costa, E. M. N. Chirwa, and S. M. Tichapondwa, *Fabrication and characterization of recyclable, magnetic ($CoFe_2O_4$)x/Ag_2S-ZnO composites for visible-light-induced photocatalytic degradation of methylene blue dye,* J. Water Process Eng. 54 (2023).
38. N. Y. Y. Lim, S. L. Chiam, C. P. Leo, and C. K. Chang, *Recent modification, mechanisms, and performance of zinc oxide-based photocatalysts for sustainable dye degradation,* Hybrid Adv. 7 (2024) 100318.